

Title page

Noninvasive evaluation of nicotinic acetylcholine receptor availability in mouse brain using
single-photon emission computed tomography with [¹²³I]5IA

Short title: [¹²³I]5IA-SPECT in the mouse brain

Yuki Matsuura¹, Masashi Ueda¹, Yusuke Higaki¹, Keiko Watanabe¹, Shogo Habara¹, Shinichiro
Kamino^{1,2}, Hideo Saji³, Shuichi Enomoto^{1,2}

¹ Department of Pharmaceutical Analytical Chemistry, Graduate School of Medicine, Dentistry, and
Pharmaceutical Sciences, Okayama University, 1-1-1 Tsushima naka, Kita-ku, Okayama 700-8530,
Japan

² Next generation Imaging Team, RIKEN Center for Life Science Technologies, 6-7-3
Minatojima-minatomachi, Chuo-ku, Kobe, Hyogo 650-0047, Japan

³ Department of Patho-Functional Bioanalysis, Graduate School of Pharmaceutical Sciences, Kyoto
University, 46-29 Yoshida Shimoadachi-cho, Sakyo-ku, Kyoto 606-8501, Japan

Corresponding author

Masashi Ueda, Ph.D.

Department of Pharmaceutical Analytical Chemistry

Graduate School of Medicine, Dentistry, and Pharmaceutical Sciences, Okayama University

E-mail: mueda@cc.okayama-u.ac.jp

Shuichi Enomoto, Ph.D.

Department of Pharmaceutical Analytical Chemistry

Graduate School of Medicine, Dentistry, and Pharmaceutical Sciences, Okayama University

E-mail: senomoto@pharm.okayama-u.ac.jp

Conflict of Interest

The authors declare that they have no conflicts of interest.

Key word

Single-photon emission computed tomography (SPECT), nicotinic acetylcholine receptor (nAChR),

mouse, 5-[¹²³I]iodo-3-(2(*S*)-azetidinylmethoxy)pyridine ([¹²³I]5IA), Tg2576, Alzheimer's disease

Abstract

Introduction

Nicotinic acetylcholine receptors (nAChRs) are of great interest because they are implicated in higher brain functions. Nuclear medical imaging is one of the useful techniques for noninvasive evaluation of physiological and pathological function in living subjects. Recent progress in nuclear medical imaging modalities enables the clear visualization of the organs of small rodents. Thus, translational research using nuclear medical imaging in transgenic mice has become possible and helps to elucidate human disease pathology. However, imaging of $\alpha 4\beta 2$ nAChRs in the mouse brain has not yet been performed. The purpose of this study was to assess the feasibility of single-photon emission computed tomography (SPECT) with 5- ^{123}I iodo-3-[2(S)-azetidylmethoxy]pyridine (^{123}I 5IA) for evaluating $\alpha 4\beta 2$ nAChR availability in the mouse brain.

Methods

A 60-min dynamic SPECT imaging session of $\alpha 4\beta 2$ nAChRs in the mouse brain was performed. The regional distribution of radioactivity in the SPECT images was compared to the density of $\alpha 4\beta 2$ nAChRs measured in an identical mouse. Alteration of nAChR density in the brains of Tg2576 mice was also evaluated.

Results

The mouse brain was clearly visualized by ^{123}I 5IA-SPECT and probe accumulation was significantly inhibited by pretreatment with (-)-nicotine. The regional distribution of radioactivity in

SPECT images showed a significant positive correlation with $\alpha 4\beta 2$ nAChR density measured in an identical mouse brain. Moreover, [^{123}I]5IA-SPECT was able to detect the up-regulation of $\alpha 4\beta 2$ nAChRs in the brains of Tg2576 transgenic mice.

Conclusions

[^{123}I]5IA-SPECT imaging would be a promising tool for evaluating $\alpha 4\beta 2$ nAChR availability in the mouse brain and may be useful in translational research focused on nAChR-related diseases.

1. Introduction

Nicotinic acetylcholine receptors (nAChRs) in the human are reported to be involved in higher brain functions such as learning, memory, and recognition [1], and to exert anxiolytic, analgesic [2], and neuroprotective effects [3, 4]. Due to the variety of functions attributed to nAChRs, their dysfunction is related to several central nervous system disorders including Alzheimer's disease (AD) [3], Parkinson's disease [5], and schizophrenia [6]. The $\alpha 4\beta 2$ subtype is one of the two predominant nAChR subtypes found in the human brain and mediates the majority of nAChR signaling [7]. Thus, elucidating how $\alpha 4\beta 2$ nAChRs are associated with physiological functions and pathological processes is of great interest.

Nuclear medical imaging technology is a procedure for *in vivo* visualization of the distribution of radioactive imaging probes using positron emission tomography (PET) and single-photon emission computed tomography (SPECT). Because this technology is noninvasive and highly quantitative [8], it enables to trace cellular and molecular events and quantify protein expression, and it is suitable for *in vivo* investigation of the molecular processes involved in physiological and pathological functions. Several imaging probes have been developed to visualize $\alpha 4\beta 2$ nAChRs *in vivo* using PET and SPECT, including 2-[^{18}F]fluoro-3-[2(*S*)-azetidylmethoxy]pyridine (^{18}F 2FA) [9], [^{18}F]nifene [10], [^{18}F]AZAN [11], [^{18}F]flubatine [12], and 5-[^{123}I]iodo-3-[2(*S*)-azetidylmethoxy]pyridine (^{123}I 5IA) [13, 14]. Noninvasive imaging of nAChRs in the human brain has been successfully performed using these

probes. These probes have also been used to demonstrate changes in nAChR availability in the brains of patients with AD [15-17] and Parkinson's disease [18], and in smokers [19].

However, the results of clinical studies are frequently complicated and often conflicting, likely due to the effects of varying combinations of symptoms and environmental factors. Some studies have reported decreased nAChR availability in AD patients [15, 16], while others have not [17]. As a complementary to clinical studies, many types of transgenic mice have recently been developed with expression of specific altered genes that relate to human diseases. Studies using transgenic mice as animal models of human disease help to elucidate the functions of mutated genes and the pathology of the resulting disease [20]. Moreover, recent improvements to the sensitivity and spatial resolution of PET and SPECT allow clear visualization of the organs of small rodents. Thus, translational research using nuclear medical imaging in transgenic mice has become possible and can provide new insight into human disease pathology. However, quantitative evaluation of $\alpha 4\beta 2$ nAChR density in the mouse brain using PET and SPECT has not yet been performed.

The present study aimed to evaluate the feasibility of SPECT imaging of $\alpha 4\beta 2$ nAChRs in the mouse brain. We selected SPECT because it is more commonly used than PET in clinical settings. We chose to use [^{123}I]5IA as a probe because it has been previously utilized for imaging of $\alpha 4\beta 2$ nAChRs and its safety and validity in rodents, non-human primates, and humans have been confirmed [21, 22]. In the present study, dynamic SPECT imaging of $\alpha 4\beta 2$ nAChRs in the mouse brain was performed and the cerebral distribution of radioactivity as determined by image analysis

was compared with the density of $\alpha 4\beta 2$ nAChRs in an identical mouse brain. *In vivo* inhibition by (-)-nicotine pretreatment was also performed to evaluate the specificity of [^{123}I]5IA binding. We also investigated whether [^{123}I]5IA-SPECT is sensitive enough to visualize and quantify neurological changes that occur in the brains of a frequently used transgenic mouse model of AD that expresses human β -amyloid precursor protein (APP) .

2. Materials and methods

2.1. Animals

Animal experiments were performed in accordance with the guidelines of the Okayama University Animal Care Committee. The experimental procedures were approved by the Okayama University Animal Care Committee. Male C57BL/6 mice (n = 29) were purchased from CLEA Japan, Inc. (Tokyo, Japan). Tg (APPSWE) 2576Kha transgenic mice (Tg2576), which express human APP containing the K670N and M671L mutations (n = 4) and age-matched wild-type littermate controls (n = 5) were also purchased from CLEA Japan, Inc.. All mice were kept at a constant ambient temperature under a 12-hour light/dark cycle with free access to food and water.

2.2. Materials

Sodium [^{123}I]iodide and sodium [^{125}I]iodide were purchased from FUJIFILM RI Pharma Co.,

Ltd. (Tokyo, Japan) and MP Biomedicals, Inc. (Santa Ana, CA, USA), respectively. The stannyl precursor of [^{123/125}I]5IA, 5-trimethylstannyl-3-[1-*tert*-butoxycarbonyl-2(*S*)-azetidylmethoxy]pyridine, was obtained from ABX GmbH (Radeberg, Germany). (-)-nicotine was purchased from Nacalai Tesque, Inc. (Kyoto, Japan). L-[*N*-methyl-³H]nicotine (80 Ci/mmol) was purchased from American Radiolabeled Chemicals Inc. (St. Louis, MO, USA). All other reagents were purchased from Wako Pure Chemical Industries, Ltd. (Osaka, Japan) and Nacalai Tesque, Inc.. Solutions were used without further purification.

2.3. Radiosynthesis

Radioiodination was performed according to a previous report [23]. Subsequent deprotection, extraction, and purification by high-performance liquid chromatography (HPLC) were performed by a previously reported method [14], except that a different column (InertSustin C18, 10 × 250 mm, GL Sciences Inc., Tokyo, Japan) and flow rate (3 mL/min) were used. After rotary evaporation of the HPLC eluent, the residue was formulated in 0.9% saline. The radiochemical purity was checked by thin-layer chromatography (chloroform/methanol/25% ammonia solution = 9/1/0.1, R_f = 0.47). The [¹²³I]5IA and [¹²⁵I]5IA were obtained with a radiochemical yield of 54% and 44%, and a radiochemical purity of > 96% and > 97%, respectively.

2.4. Biodistribution in mice

C57BL/6 mice (n = 4) received injections of [¹²⁵I]5IA (150 kBq) via the tail vein. The mice were killed by decapitation at 5, 15, 30, and 60 min after the injection. The brains were immediately harvested and divided into five regions (thalamus, cerebellum, striatum, hippocampus, and cortex). The divided regions were weighed and their radioactivity was measured by a gamma counter (AccuFLEX γ , Hitach Aloka Medical, Ltd., Tokyo, Japan). The results were expressed as the percentage injected dose per gram tissue (%ID/g).

2.5. SPECT study in C57BL/6 mice

2.5.1. Dynamic SPECT/CT imaging

SPECT/CT imaging was performed by using a Triumph SPECT2/CT (TriFoil Imaging., Chatsworth, CA, USA) with specially designed multi-pinhole collimators (75A10). The energy window was $\pm 20\%$ and centered on the iodine-123 photopeak (159 keV) with a cadmium zinc telluride (CZT) detector. SPECT images were acquired in continuous rotation mode with 16 projections per camera for 360° and 40 s per projection with a 35 mm radius of rotation. The resolution and sensitivity was 0.8-mm full width at half maximum and 99.1 count/sec/MBq, respectively. A 3D-ordered subset expectation maximization (3D-OSEM) algorithm was applied using eight subsets and five iterations in FLEX-RECON software for multi-pinhole SPECT imaging. Images were reconstructed in $256 \times 256 \times 256$ matrix size with dimensions of $0.75 \times 0.75 \times 0.75$

mm. CT data were acquired at a 512×512 matrix size image representing a 91.3 mm field-of-view and 0.38 mm slice thickness. The tube voltage and current were set at 75 kV and 140 μ A, respectively. All CT imaging data were reconstructed using a filtered back-projection algorithm with a ramp filter. The reconstructed pixels were $0.38 \times 0.38 \times 0.38$ mm in the x, y, and z dimensions.

[123 I]5IA (8.2–12.3 MBq) was injected into each C57BL/6 mouse (n = 5) via the tail vein under awake conditions and the mice were anesthetized with 3% isoflurane in an anesthetic box immediately after injection. Each mouse was placed in a mouse imaging chamber and a 4-min CT scan was performed approximately 5 min after the injection. SPECT data were acquired approximately 10 min after injection by 4 sets of 10-min scans. Since it took 2 min for the CZT detectors to return to their original position after the scan finished, the total operating time of each scan set was 12 min. The mouse was maintained at 1.5% isoflurane anesthesia throughout the scans. After the SPECT/CT scans, the mice were returned to their cages and kept for 7 days to attenuate the radioactivity of 123 I sufficiently. Then, the mice was used for the autoradiographic studies.

2.5.2. *Magnetic resonance imaging*

Each mouse was subjected to magnetic resonance (MR) brain imaging on the day prior to the SPECT study. The MRI scans were performed using a 4.7 Tesla BioSpec (Bruker BioSpin, Ettlingen, Germany). Three-dimensional T2-weighted images were acquired using a fast spin echo sequence. The following parameters were used: repetition time = 2000 ms, echo time = 65 ms,

number of averages = 2, flip angle = 90°, field-of-view = 18 × 15 × 10 mm, resolution = 125 μm, and slice thickness = 1.0 mm. The mice were maintained at 1.5% isoflurane anesthesia throughout the scans.

2.5.3. Image analysis

The level of radioactivity accumulation within each brain region was determined by a region-of-interest (ROI) method using PMOD software ver. 3 (PMOD Technologies Ltd., Zurich, Switzerland). For ROI definition, the MR image was coregistered to each CT image using an automatic rigid matching tool with manual adjustment when needed. Two spheroidal ROIs in each region were symmetrically placed on the MR images, saved with a transformation matrix, and then applied to SPECT images in the following brain regions: thalamus (1.6 mm in diameter), cerebellum (1.6 mm in diameter), striatum (1.6 mm in diameter), cerebral cortex (1.6 mm in diameter), and hippocampus (1.0 mm in diameter). The mean radioactivity for each ROI was given as the midpoint of each of the 16-projection sequences. The mean radioactivity (count/voxel) was then converted to kBq/cc using a calibration factor of 0.014 for the 40-s-per-projection scan. These factors were determined by phantom scans of a 2 mL plastic tube filled with the same ¹²³I solution used in the acquisition and reconstruction of data and according to the same protocol as the mouse imaging study. Standardized uptake values (SUVs) were calculated according to the following equation: SUV = radioactivity for each ROI (kBq/cc) / (injected dose [kBq] / body weight [g]) × 100.

2.6. Autoradiographic analysis of nAChR density in the mouse brain

Animals were killed 7 days after dynamic SPECT/CT imaging, and the brains were rapidly removed and frozen in a mixture of dry-ice and hexane (-75°C) until sectioning. Ten-micrometer-thick sections were cut on a Microm HM 505 E cryostat (GMI, Inc., Ramsey, MN, USA) and mounted on glass slides. The slides were dried at room temperature overnight and then stored at -80°C until use.

The binding of [³H]nicotine was measured using a modification of the procedure of Pauly *et al.* [24]. After preincubation in 20 mM Krebs-Ringer HEPES buffer (pH 7.4) for 30 min at 4°C, the sections were incubated with 4 nM [³H]nicotine in Krebs-Ringer HEPES buffer for 90 min at 4°C. Non-specific binding was measured in adjacent serial sections by incubation with 100 μM (-)-nicotine. Next, the sections were washed with Krebs-Ringer HEPES buffer for 3 min (3 × 1 min) at 4°C. The sections were rapidly air-dried, and then exposed to a tritium-sensitive imaging plate (Fuji Imaging Plate BAS-TR; Fuji Photo Film, Tokyo, Japan) along with a tritium standard (ART 0123; American Radiolabeled Chemicals Inc.) for 20 h.

The imaging plate was scanned using an FLX-7000 scanner (Fuji Photo Film), and the resulting autoradiograms were quantitatively analyzed using Multi Gauge ver. 3 software (Fuji Photo Film). Two independent measurements were taken from the thalamus, cerebellum, striatum, cerebral cortex, and hippocampus of five mice, identified using a mouse brain atlas [25]. [³H]nicotine binding

(fmol/mg wet weight) was calculated for each measurement after calculating the radioactive intensity (nCi/mg) using a standard curve obtained from images of the tritium standard. To determine the specific binding, non-specific binding in adjacent serial sections was subtracted from the total binding in each region.

2.7. Nicotine treatment study

SPECT/CT imaging were performed twice in C57BL/6 mice (n = 4). In the baseline study, [¹²³I]5IA (9.3–12.6 MBq) was injected into the tail vein after subcutaneous injection of saline (100 μL). The inhibition study was performed 7 days after the baseline study when the radioactivity had sufficiently attenuated. In the inhibition study, (-)-nicotine (10 mg/kg) was subcutaneously injected, and 5 min later [¹²³I]5IA (9.2–11.2 MBq) was injected into the tail vein. In both studies, a single set of 30-min SPECT scans of brain was performed 45 min after the injection of [¹²³I]5IA, followed by a 5-min CT scan. The mice were maintained at 1.5% isoflurane anesthesia throughout the scans. SPECT images were acquired using 16 projections per camera for 360° and 120 s per projection. The obtained mean radioactivity (count/voxel) was converted to kBq/cc using a calibration factor 0.039 for the 120-s-per-projection scan. MR imaging and image analysis were performed in the same way as described in the *section 2.5*.

2.8. SPECT study in Tg2576 mice

A 60-min dynamic SPECT imaging was performed in Tg2576 mice and littermate wild-type mice (13 months of age, n = 4–5 per group, [^{123}I]5IA dose; 8.1–12.9 MBq). MR imaging and image analysis were performed in the same way as described in the *section 2.5*. After completion of scans, the mice were returned to their cages and kept for 7 days to allow attenuation of radioactivity. Seven days after SPECT/CT imaging, each mouse was killed and the binding of [^3H]nicotine was measured using the same protocol as in the *section 2.6*.

2.9. Statistical analysis

GraphPad Prism ver. 5 (GraphPad, San Diego, CA, USA) was used for all statistical analyses. Correlation coefficients were assessed using Pearson's analysis. Paired *t*-tests were used to compare data between the baseline and (-)-nicotine-treated SPECT studies. The other comparisons between two groups were performed with student's *t*-test. A *P* value < 0.05 was considered to be statistically significant. All data are expressed as mean \pm standard deviation (SD).

3. Results

3.1. Dynamic SPECT imaging and biodistribution after injection of [$^{123/125}\text{I}$]5IA

Fig. 1a shows representative coronal MR images and SPECT/CT images of mouse brain obtained 18, 33, 48, and 62 min after injection of [^{123}I]5IA. The upper images show slices at the level

of the thalamus, which is a nAChR-rich region. The lower images show images at the level of the cerebellum which is a nAChR-poor region. The radioactive signal was distributed across nearly the whole brain in both slices 18 min after injection. At the cerebellar level, the radioactive signal was rapidly cleared in a time-dependent manner. In contrast, the signal at the thalamic level lasted until 62 min after injection of [^{123}I]5IA. The time-activity curves of the five brain regions were generated using ROI analyses and are shown in Fig. 1b. The times at which each SUV is given in Fig. 1b are 16, 31, 45, and 60 min, expressed as the average of the imaging midpoints of 5 mice. Radioactive signal was highest in the thalamus, followed by the striatum, hippocampus, cortex, and cerebellum. With the exception for the thalamus, each region showed a peak signal 16 min after injection, followed by gradual clearance. In the thalamus, [^{123}I]5IA signal increased until 31 min after injection and then gradually decreased. In the biodistribution study, the radioactive signal was highest in the thalamus, with slightly lower levels in the striatum, hippocampus, and cerebral cortex, and the lowest levels in the cerebellum (Fig. 1c). These orders were in accordance with the SPECT study.

3.2. Comparison of in vivo SPECT analysis with autoradiographic analysis of nAChR density determined in an identical mouse brain

The density of $\alpha 4\beta 2$ nAChRs in each brain region as determined by [^3H]nicotine autoradiography was in accordance with a previous report [24]. In our preliminary biodistribution analysis, the brain-to-blood ratio increased in a time-dependent manner and the highest value was

obtained 60 min after [¹²⁵I]5IA injection among the time points examined (5–60 min). Therefore, we compared SUVs 60 min after injection with the density of α4β2 nAChRs indicated by [³H]nicotine binding. The *in vivo* SPECT signal accumulation as determined by the ROI method showed a significant positive correlation with [³H]nicotine binding measured in an identical mouse brain (Fig. 2a, R = 0.55, P < 0.005 at 60 min). Moreover, the binding potential ratios (BPR = radioactivity in a target region / radioactivity in the cerebellum) [26] calculated using the data obtained 60 min after the [¹²³I]5IA injection showed a positive correlation with α4β2 nAChR density (Fig. 2b, R = 0.45, P < 0.01 at 60 min).

3.3. Effect of nicotine pretreatment on [¹²³I]5IA SPECT images

Fig. 3a shows thalamic SPECT/CT images of baseline and nicotine treatment studies obtained 60 min after injection of [¹²³I]5IA. Compared to baseline conditions (Fig. 3a, *left image*), radioactivity accumulation was significantly decreased by pretreatment with (-)-nicotine (Fig. 3a, *right image*). As shown in Fig. 3b, pretreatment with (-)-nicotine reduced radioactivity accumulation by 43%, 31%, 27%, and 23% in the thalamus, striatum, hippocampus, and cortex, respectively. In contrast, nicotine pretreatment did not result in significant signal reduction in the cerebellum.

3.4. Changes in [¹²³I]5IA binding and nAChR density in mouse model of Alzheimer's disease

[¹²³I]5IA-SPECT of brains of Tg2576 mice showed higher signal accumulation compared to wild-type littermate controls (Fig. 4a). This finding is consistent with the increase in [³H]nicotine binding in the brains of Tg2576 mice (Fig. 4b). In particular, [¹²³I]5IA accumulation in the thalamus was significantly increased compared to wild-type mice (22%, $P < 0.05$). Similarly, [³H]nicotine binding in the thalamus showed a significant increase in Tg2576 compared to wild-type mice (28%, $P < 0.05$). These results suggest that nAChRs are up-regulated in the Tg2576 mouse brain.

4. Discussion

The present study provides the first evaluation of SPECT imaging of $\alpha 4\beta 2$ nAChRs in the mouse brain. The living mouse brain was clearly visualized and levels of radioactivity accumulation in each brain region, as determined by ROI analysis, showed a significant positive correlation with $\alpha 4\beta 2$ nAChR density determined in an identical mouse brain. Pretreatment with (-)-nicotine significantly inhibited the accumulation of [¹²³I]5IA in the brain. These results indicate that the [¹²³I]5IA-SPECT signal was specific to $\alpha 4\beta 2$ nAChRs, and that [¹²³I]5IA-SPECT signal intensity can be used as an indicator of $\alpha 4\beta 2$ nAChR density. The extent of the decrease in radioactivity after nicotine treatment was lower than in a previous study [23], and could be attributable to an effect of anesthesia. It was reported that higher radioactivity was accumulated in the brain under isoflurane anesthesia compared with the conscious condition [27]. Therefore, slow clearance of [¹²³I]5IA from

the brain under isoflurane anesthesia could cause the low baseline/blocking ratios compared to the previous study that was performed in the conscious condition. Furthermore, up-regulation of $\alpha 4\beta 2$ nAChRs in Tg2576 mice could be detected by SPECT/CT imaging with [^{123}I]5IA. Therefore, [^{123}I]5IA-SPECT will be a useful tool for *in vivo* investigation of altered $\alpha 4\beta 2$ nAChR expression in transgenic mice with genes modifications related to human diseases.

Due to the small size of the mouse brain and the close proximity between regions, precise placement of ROIs is important. For this purpose, co-registration of MR and SPECT/CT images was performed using the skulls and orbits as references. ROIs were placed on MR images, and then applied to SPECT images. To avoid underestimation of radioactive signal due to partial volume effects, the radius of the spheroidal ROIs was varied to fit the anatomical size of each region. Despite these precautions, the radioactivity in a region may be overestimated if high radioactivity accumulates in an adjacent regions, such as in the case of the Harderian gland [28]. In this study, the hippocampus and striatum's anatomically close position to the thalamus, which showed significant radioactivity accumulation, is concerned. Although radioactivity accumulation as determined by the dissection method in the cortex, striatum, and hippocampus were nearly the same level, SUVs in the striatum and hippocampus were higher than those in the cortex, suggesting an effect of radioactivity in the thalamus on these neighboring regions. However, it should be noted that a significant positive correlation was observed between SPECT signal intensity and nAChR density regardless of whether the striatum and hippocampus were included (Fig. 2a) or excluded ($R = 0.75$, $P < 0.005$ at 60 min,

data not shown).

In the present study, we used [³H]nicotine as a radioligand to determine $\alpha 4\beta 2$ nAChR density in the mouse brain. Although [³H]nicotine has an affinity not only to $\alpha 4\beta 2$ nAChRs, but also to $\alpha 3\beta 2$ and $\alpha 3\beta 4$ nAChRs [29], in rodent brains, more than 72% of nAChRs were found to be of the $\alpha 4\beta 2$ subtype in the 4 regions evaluated in this study, except in the cerebellum [30]. Therefore, [³H]nicotine binding would be mainly attributable to $\alpha 4\beta 2$ nAChRs and could be used as an index of $\alpha 4\beta 2$ nAChR density, at least in the cortex, striatum, hippocampus, and thalamus. In the cerebellum, since 51% of nAChRs was of the $\alpha 4\beta 2$ subtype and 49% was of the $\alpha 3\beta 4$ subtype, $\alpha 4\beta 2$ nAChR density might be overestimated if judged from the [³H]nicotine binding. However, the effect of overestimation would be limited because the cerebellum is a nAChR-poor region (only one-fifth to one-third of [¹²⁵I]5IA binding compared with the other 4 regions).

A limitation of the present study is the lack of kinetic analyses of the SPECT imaging data. In human and non-human primates, tracer kinetic analyses using imaging and blood sampling techniques have been performed to calculate distribution volume or binding potential of tracers [22, 31]. However, in the case of mice, it is difficult to collect arterial blood constantly throughout a PET/SPECT scan because of their small blood volume. It is possible to calculate receptor density without blood sampling if a reference region in the brain is used that lacks expression of an imaging target. For example, Okada *et al.*, used the corpus callosum as a reference region to calculate the binding potential of [¹⁸F]2FA, revealing low availability of nAChRs in patients with AD [32].

However, this method cannot be applied in small animal SPECT imaging because the spatial resolution of SPECT is not high enough to distinguish the corpus callosum from other regions. Pretreatment with (-)-nicotine did not affect [^{123}I]5IA accumulation in the cerebellum, suggesting that the cerebellum may be used as a reference region when using this probe in the mouse brain. In our SPECT study, BPR calculated using the data obtained 60 min after the [^{123}I]5IA injection showed a positive correlation with $\alpha 4\beta 2$ nAChR density (Fig. 2b). Other researchers have calculated the BPR using the cerebellum as a reference region in the rat brain [33]. Therefore, semi-quantitative analysis of nAChR density may be possible using PET/SPECT imaging in rodent brains, though further validation will be necessary.

SPECT is more widely available than PET in clinical settings. This is a significant advantage for the use of nuclear medical imaging in translational research. Although SPECT is less quantitative than PET, techniques have recently been developed to increase its quantitative capacity, such as algorithms to improve the quality of reconstructed images [34] and methods for the precise correction of attenuation and scattering effects [35, 36]. In addition to these techniques, improvement in the sensitivity and spatial resolution of SPECT will increase its quantitative capability in the future.

Tg2576 transgenic mice expressing the human APP with K670N and M671L mutations show early phenotypic changes which may reflect AD pathology such as elevation of $\text{A}\beta_{1-40/1-42}$ levels, presence of amyloid plaques, and memory and learning defects [37]. A previous autoradiography

study showed a significant increase in accumulations of [³H]cytisine in the thalamus of 11-month-old Tg2576 mice [38]. We examined whether [¹²³I]5IA-SPECT is adequately sensitive to detect nAChR up-regulation in the brain of Tg2576 mice. We found a significant increase in accumulation of [¹²³I]5IA in the thalamus of 13-month-old Tg2576 mice compared to wild-type littermate controls. Therefore, we conclude that [¹²³I]5IA-SPECT is sufficiently sensitive to assess changes in nAChRs in the brain of a mouse model of AD. In contrast to our findings, several studies have reported a decrease in nAChR availability in AD patients [15, 16]. The reason for this discrepancy in $\alpha 4\beta 2$ nAChR expression between Tg2576 mice and AD patients is unclear. It is possible that the phenotype of Tg2576 mice represents a pre-AD state. This hypothesis is supported by observation of resting-state cerebral hypermetabolism in Tg2576 mice [39] and early-onset AD patients [40], but not in patients with advanced AD [41]. Furthermore, no significant differences were found between Tg2576 and wild-type mice at 12-13 months of age in novel object recognition memory (data not shown) or plaque deposition [42]. Therefore, up-regulation of $\alpha 4\beta 2$ nAChRs may play a role in mechanisms underlying neurodegeneration in early-stage AD patients with increased A β expression. Overall, these results will motivate further studies that focus on nAChR availability in transgenic mouse model of nAChR-related human disease. *In vivo* [¹²³I]5IA-SPECT in mouse models may help to elucidate the mechanisms underlying changes in nAChR expression as the disease advances or to perform image-based screening of nAChR-targeting drugs.

5. Conclusion

The mouse brain was clearly visualized using [^{123}I]5IA-SPECT. Probe accumulation was significantly inhibited by pretreatment with (-)-nicotine. The regional distribution of radioactivity in SPECT images showed significant positive correlation with $\alpha 4\beta 2$ nAChR density determined in an identical mouse brain. Moreover, [^{123}I]5IA-SPECT could detect up-regulation of $\alpha 4\beta 2$ nAChRs in the brain of Tg2576 mice. Thus, the present study indicates that [^{123}I]5IA-SPECT provides an accurate assessment of $\alpha 4\beta 2$ nAChR density in the mouse brain. To our knowledge, this is the first report to demonstrate that [^{123}I]5IA-SPECT is a suitable tool for noninvasive measurement of $\alpha 4\beta 2$ nAChR availability in the mouse brain. This technique may be useful for translational research of nAChR-related diseases and image-based screening of nAChR-targeting drugs.

References

- [1] Levin ED and Simon BB. Nicotinic acetylcholine involvement in cognitive function in animals. *Psychopharmacology* 1998;138:217-30.
- [2] Ueda M, Iida Y, Tominaga A, Yoneyama T, Ogawa M, Magata Y, *et al.* Nicotinic acetylcholine receptors expressed in the ventralposterolateral thalamic nucleus play an important role in anti-allodynic effects. *Br J Pharmacol* 2010;159:1201-10.
- [3] Dani JA and Bertrand D. Nicotinic acetylcholine receptors and nicotinic cholinergic mechanisms of the central nervous system. *Annu Rev Pharmacol Toxicol* 2007;47:699-729.
- [4] Ueda M, Iida Y, Kitamura Y, Kawashima H, Ogawa M, Mayata Y, *et al.* 5-Iodo-A-85380, a specific ligand for alpha A beta 2 nicotinic acetylcholine receptors, prevents glutamate neurotoxicity in rat cortical cultured neurons. *Brain Res* 2008;1199:46-52.
- [5] Quik M and Wonnacott S. alpha 6 beta 2*and alpha 4 beta 2*nicotinic acetylcholine receptors as drug targets for Parkinson's disease. *Pharmacol Rev* 2011;63:938-66.
- [6] Breese CR, Lee MJ, Adams CE, Sullivan B, Logel J, Gillen KM, *et al.* Abnormal regulation of high affinity nicotinic receptors in subjects with schizophrenia. *Neuropsychopharmacology* 2000;23:351-64.
- [7] Alkondon M and Albuquerque EX. Nicotinic acetylcholine receptor alpha 7 and alpha 4 beta 2 subtypes differentially control GABAergic input to CA1 neurons in rat hippocampus. *J Neurophysiol* 2001;86:3043-55.

- [8] Ichise M, Meyer JH, and Yonekura Y. An introduction to PET and SPECT neuroreceptor quantification models. *J Nucl Med* 2001;42:755-63.
- [9] Kimes AS, Chefer SI, Matochik JA, Contoreggi CS, Vaupel DB, Stein EA, *et al.* Quantification of nicotinic acetylcholine receptors in the human brain with PET: Bolus plus infusion administration of 2- F-18 F-A85380. *Neuroimage* 2008;39:717-27.
- [10] Pichika R, Easwaramoorthy B, Collins D, Christian BT, Shi BZ, Narayanan TK, *et al.* Nicotinic alpha 4 beta 2 receptor imaging agents - Part II. Synthesis and biological evaluation of 2- F-18 fluoro-3-[2-((S)-3-pyrrolinyl)methoxy]pyridine (F-18-nifene) in rodents and imaging by PET in nonhuman primate. *Nucl Med Biol* 2006;33:295-304.
- [11] Wong DF, Kuwabara H, Kim J, Bragsic JR, Chamroonrat W, Gao YJ, *et al.* PET Imaging of High-Affinity alpha 4 beta 2 Nicotinic Acetylcholine Receptors in Humans with F-18-AZAN, a Radioligand with Optimal Brain Kinetics. *J Nucl Med* 2013;54:1308-14.
- [12] Sabri O, Becker GA, Meyer PM, Hesse S, Wilke S, Graef S, *et al.* First-in-human PET quantification study of cerebral alpha 4 beta 2*nicotinic acetylcholine receptors using the novel specific radioligand (-)- F-18 Flubatine. *Neuroimage* 2015;118:199-208.
- [13] Ueda M, Iida Y, Mukai T, Mamede M, Ishizu K, Ogawa M, *et al.* 5- I-123 iodo-A-85380: assessment of pharmacological safety, radiation dosimetry and SPECT imaging of brain nicotinic receptors in healthy human subjects. *Ann Nucl Med* 2004;18:337-44.
- [14] Saji H, Ogawa M, Ueda M, Iida Y, Magata Y, Tominaga A, *et al.* Evaluation of radioiodinated

5-iodo-3-(2(S)-azetidinylmethoxy)pyridine as a ligand for SPECT investigations of brain nicotinic acetylcholine receptors. *Ann Nucl Med* 2002;16:189-200.

[15] O'Brien JT, Colloby SJ, Pakrasi S, Perry EK, Pimlott SL, Wyper DJ, *et al.* alpha 4 beta 2 nicotinic receptor status in Alzheimer's disease using I-123-5IA-85380 single-photon-emission computed tomography. *J Neurol Neurosurg Psychiatry* 2007;78:356-62.

[16] Terriere E, Sharman M, Donaghey C, Herrmann L, Lonie J, Strachan M, *et al.* alpha 4 beta 2-nicotinic receptor binding with 5-IA in Alzheimer's disease: Methods of scan analysis. *Neurochem Res* 2008;33:643-51.

[17] Mitsis EM, Reech KM, Bois F, Tamagnan GD, MacAvoy MG, Seibyl JP, *et al.* I-123-5-IA-85380 SPECT Imaging of Nicotinic Receptors in Alzheimer Disease and Mild Cognitive Impairment. *J Nucl Med* 2009;50:1455-63.

[18] Oishi N, Hashikawa K, Yoshida H, Ishizu K, Ueda M, Kawashima H, *et al.* Quantification of nicotinic acetylcholine receptors in Parkinson's disease with I-123-5IA SPECT. *J Neurol Sci* 2007;256:52-60.

[19] Wuellner U, Guendisch D, Herzog H, Minnerop M, Joe A, Warnecke M, *et al.* Smoking upregulates alpha 4 beta(2)* nicotinic acetylcholine receptors in the human brain. *Neurosci Lett* 2008;430:34-7.

[20] Shultz LD, Ishikawa F, and Greiner DL. Humanized mice in translational biomedical research. *Nat Rev Immunol* 2007;7:118-30.

- [21] Mamede M, Ishizu K, Ueda M, Mukai T, Iida Y, Fukuyama H, *et al.* Quantification of human nicotinic acetylcholine receptors with ^{123}I -5IA SPECT. *J Nucl Med* 2004;45:1458-70.
- [22] Fujita M, Tamagnan G, Zoghbi SS, Al-Tikriti MS, Baldwin RM, Seibyl JP, *et al.* Measurement of alpha(4)beta(2) nicotinic acetylcholine receptors with I-123 5-I-A-85380 SPECT. *J Nucl Med* 2000;41:1552-60.
- [23] Horti AG, Koren AO, Lee KS, Mukhin AG, Vaupel DB, Kimes AS, *et al.* Radiosynthesis and preliminary evaluation of 5- I-123/125 iodo3-(2(S)-azetidylmethoxy)pyridine: A radioligand for nicotinic acetylcholine receptors. *Nucl Med Biol.* 1999;26:175-82.
- [24] Pauly JR, Marks MJ, Robinson SF, vandeKamp JL, and Collins AC. Chronic nicotine and mecamylamine treatment increase brain nicotinic receptor binding without changing alpha 4 or beta 2 mRNA levels. *J Pharmacol Exp Ther* 1996;278:361-9.
- [25] George Paxinos and Franklin KBJ. Paxinos and Franklin's the Mouse Brain in Stereotaxic Coordinates, Fourth Edition, 2012.
- [26] Logan J, Fowler JS, Volkow ND, Wang GJ, Ding YS, and Alexoff DL. Distribution volume ratios without blood sampling from graphical analysis of PET data. *J Cereb Blood Flow Metab* 1996;16:834-40.
- [27] Baba JS, Endres CJ, Foss CA, Nimmagadda S, Jung H, Goddard JS, *et al.* Molecular Imaging of Conscious, Unrestrained Mice with AwakeSPECT. *J Nucl Med* 2013;54:969-76.
- [28] Kim M, Woo S-K, Yu JW, Lee YJ, Kim KM, Kang JH, *et al.* Effect of Harderian adenectomy on

the statistical analyses of mouse brain imaging using positron emission tomography. *J Vet Sci* 2014;15:157-61.

[29] Jensen AA, Frolund B, Lijefors T, and Krogsgaard-Larsen P. Neuronal nicotinic acetylcholine receptors: Structural revelations, target identifications, and therapeutic inspirations. *J Med Chem* 2005;48:4705-45.

[30] Perry DC, Xiao YX, Nguyen HN, Musachio JL, Davila-Garcia MI, and Kellar KJ. Measuring nicotinic receptors with characteristics of alpha 4 beta 2, alpha 3 beta 2 and alpha 3 beta 4 subtypes in rat tissues by autoradiography. *J Neurochem* 2002;82:468-81.

[31] Price JC. Principles of tracer kinetic analysis. *Neuroimaging Clin N Am* 2003;13:689-704.

[32] Okada H, Ouchi Y, Ogawa M, Futatsubashi M, Saito Y, Yoshikawa E, *et al.* Alterations in alpha 4 beta 2 nicotinic receptors in cognitive decline in Alzheimer's aetiopathology. *Brain* 2013;136:3004-17.

[33] Bieszczad KM, Kant R, Constantinescu CC, Pandey SK, Kawai HD, Metherate R, *et al.* Nicotinic acetylcholine receptors in rat forebrain that bind ^{18}F -nifene: Relating PET imaging, autoradiography, and behavior. *Synapse* 2012;66:418-34.

[34] Zoccarato O. Innovative reconstruction algorithms in cardiac SPECT scintigraphy. *Q J Nucl Med Mol Imaging* 2012;56:230-46.

[35] Larsson A, Johansson L, Sundstrom T, and Ahlstrom KR. A method for attenuation and scatter correction of brain SPECT based on computed tomography images. *Nucl Med Commun*

2003;24:411-20.

[36] Romer W, Fiedler E, Pavel M, Pfahlberg A, Hothorn T, Herzog H, *et al.* Attenuation correction of SPECT images based on separately performed CT - Effect on the measurement of regional uptake values. *Nuklearmedizin* 2005;44:20-8.

[37] Webster SJ, Bachstetter AD, Nelson PT, Schmitt FA, and Eldik LJV. Using mice to model Alzheimer's dementia: an overview of the clinical disease and the preclinical behavioral changes in 10 mouse models. *Front Genet* 2014;23:1-23.

[38] Bednar I, Paterson D, Marutle A, Pham TM, Svedberg M, Hellstrom-Lindahl E, *et al.* Selective nicotinic receptor consequences in APP(SWE) transgenic mice. *Mol Cell Neurosci* 2002;20:354-65.

[39] Luo F, Rustay NR, Ebert U, Hradil VP, Cole TB, Llano DA, *et al.* Characterization of 7- and 19-month-old Tg2576 mice using multimodal in vivo imaging: limitations as a translatable model of Alzheimer's disease. *Neurobiol Aging* 2012;33:933-44.

[40] Cohen AD, Price JC, Weissfeld LA, James J, Rosario BL, Bi WZ, *et al.* Basal Cerebral Metabolism may modulate the cognitive effects of a-beta in mild cognitive impairment: an example of brain reserve. *J Neurosci* 2009;29:14770-8.

[41] Choo IH, Lee DY, Youn JC, Jhoo JH, Kim KW, Lee DS, *et al.* Topographic patterns of brain functional impairment progression according to clinical severity staging in 116 Alzheimer disease patients: FDG-PET study. *Alzheimer Dis Assoc Disord* 2007;21:77-84.

[42] Jacobsen JS, Wu CC, Redwine JM, Comery TA, Arias R, Bowlby M, *et al.* Early-onset

behavioral and synaptic deficits in a mouse model of Alzheimer's disease. Proc Natl Acad Sci USA 2006;103:5161-6.

Acknowledgments

The authors are grateful to Okayama Medical Innovation Center for assistance with image analyses. This work was supported in part by a Grant-in-Aid for COE projects by MEXT, Japan, titled "Center of excellence for molecular and gene targeting therapies with micro-dose molecular imaging modalities", a Grant-in-Aid for Challenging Exploratory Research (KAKENHI No. 26670562) from the Japan Society for the Promotion of Science, and a grant from the Smoking Research Foundation.

Figure 1

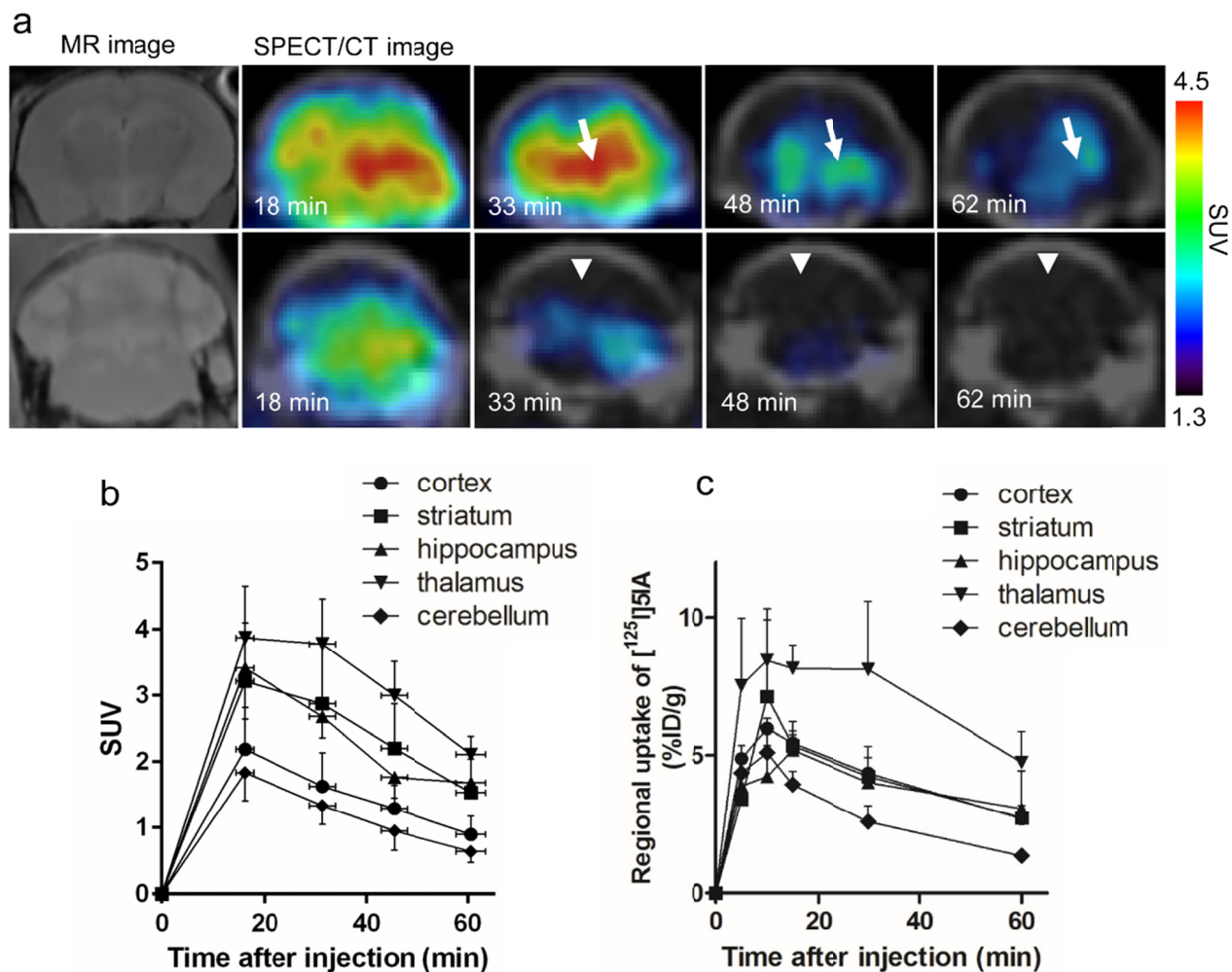


Figure 1. Dynamic SPECT imaging and biodistribution after injection of [^{123/125}I]5IA

(a) Representative MR and SPECT/CT images obtained 18, 33, 48, and 62 min after injection of [¹²³I]5IA (27.3 MBq). Upper and lower images show slices at the thalamic and cerebellar levels, respectively. Arrows indicate the thalamus and arrowheads indicate the cerebellum. The color bar indicates the level of radioactivity accumulation of [¹²³I]5IA (SUV). The mouse was maintained at 1.5% isoflurane anesthesia throughout the scans. (b) *In vivo* time-activity curves of [¹²³I]5IA-SPECT

signal in the indicated brain regions. Each point represents the mean \pm SD for 5 mice. (c) Cerebral regional uptakes of [125 I]5IA (%ID/g) after intravenous administration as determined by the dissection method. Each point represents the mean \pm SD for 4 mice.

Figure 2

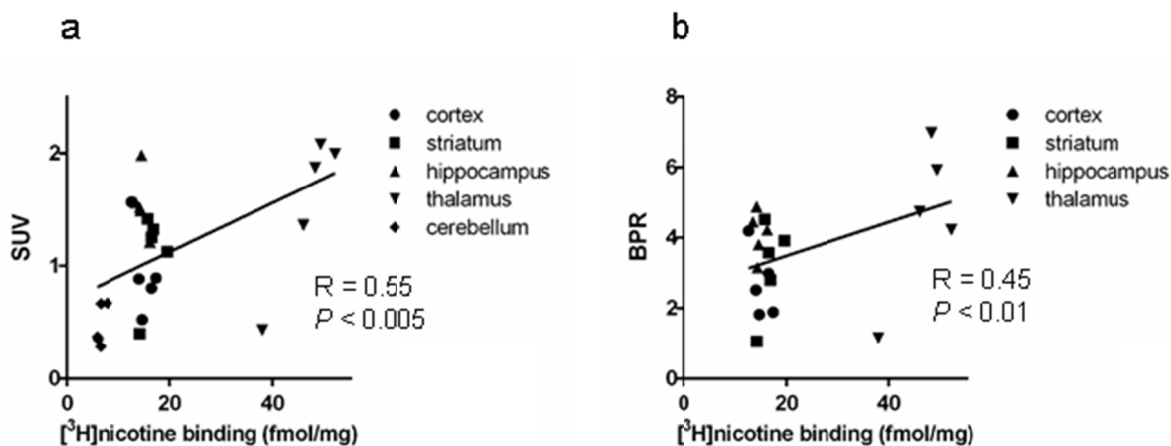


Figure 2. Comparison of in vivo SPECT analysis with autoradiographic analysis of nAChR density determined in an identical mouse brain

(a) Y-axes indicate SUVs in each brain region obtained 60 min after injection of $[^{123}\text{I}]5\text{IA}$. X-axes represent $\alpha 4\beta 2$ nAChR density as determined by $[^3\text{H}]$ nicotine binding assay. The correlation coefficient (R) was 0.55 (n=5), indicating a significant correlation between the two parameters ($P < 0.005$). (b) Y-axes indicate BPR in each brain region obtained 60 min after injection of $[^{123}\text{I}]5\text{IA}$. X-axes represent $\alpha 4\beta 2$ nAChR density as determined by $[^3\text{H}]$ nicotine binding assay. The correlation coefficient (R) was 0.45 (n=5), indicating a significant correlation between the two parameters ($P < 0.01$).

Figure 3

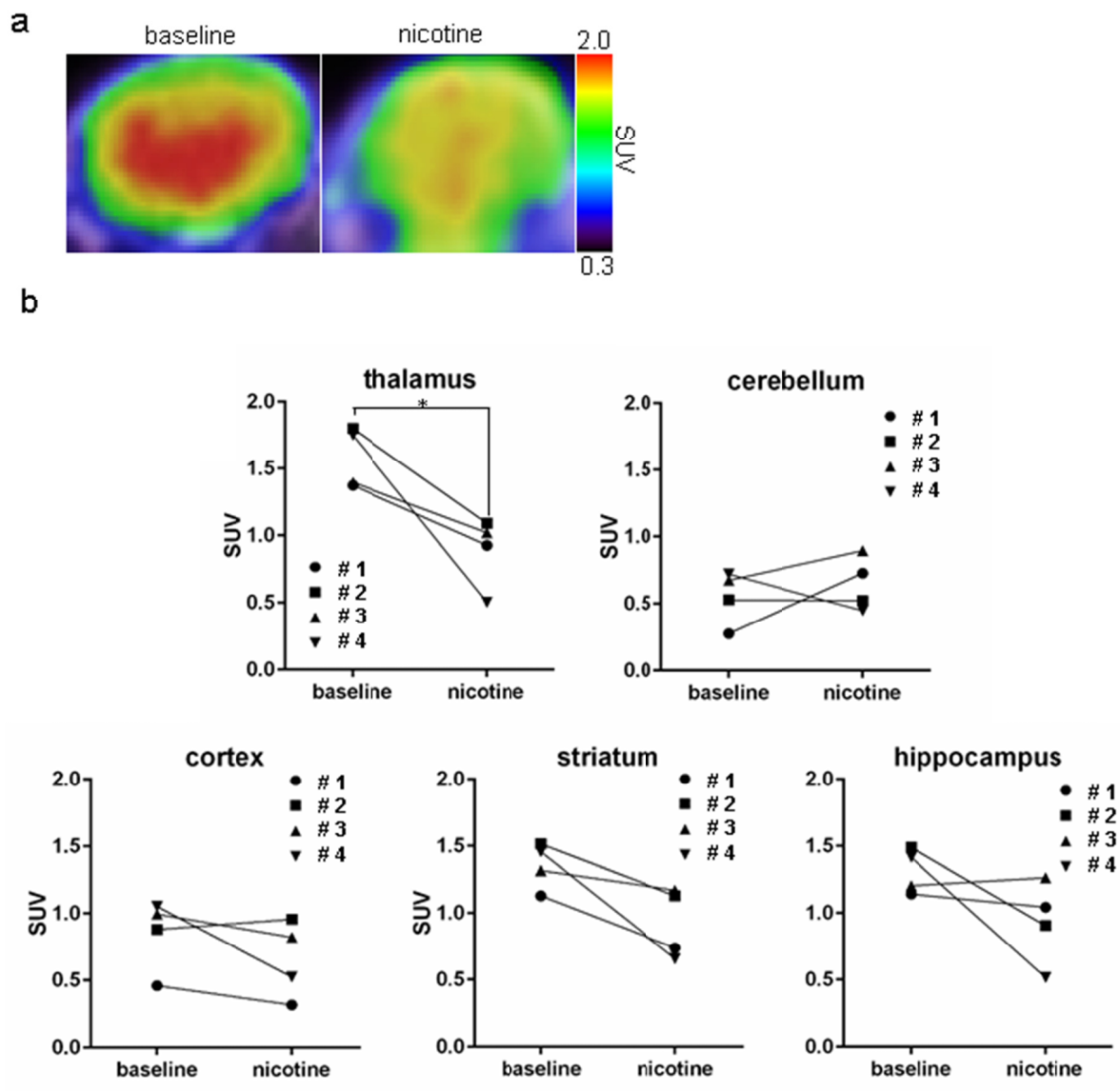


Figure 3. Effect of nicotine pretreatment on [¹²³I]5IA SPECT images

(a) Representative SPECT/CT images at the thalamic level obtained 60 min after the injection of [¹²³I]5IA in the baseline study (*left*) and the (-)-nicotine pretreatment study (*right*). The colored bar indicates the level of radioactivity accumulation of [¹²³I]5IA (SUV). The mouse was maintained at

1.5% isoflurane anesthesia throughout the scans. (b) Effects of pretreatment with (-)-nicotine (10 mg/kg) on binding of [¹²³I]5IA in each brain region (n=4, individual identification number # 1 - 4). Y-axes indicate SUVs in the baseline and (-)-nicotine treatment studies in each brain region. Pretreatment with (-)-nicotine significantly reduced radioactivity accumulation in the thalamus ($P < 0.05$ vs. baseline study).

Figure 4

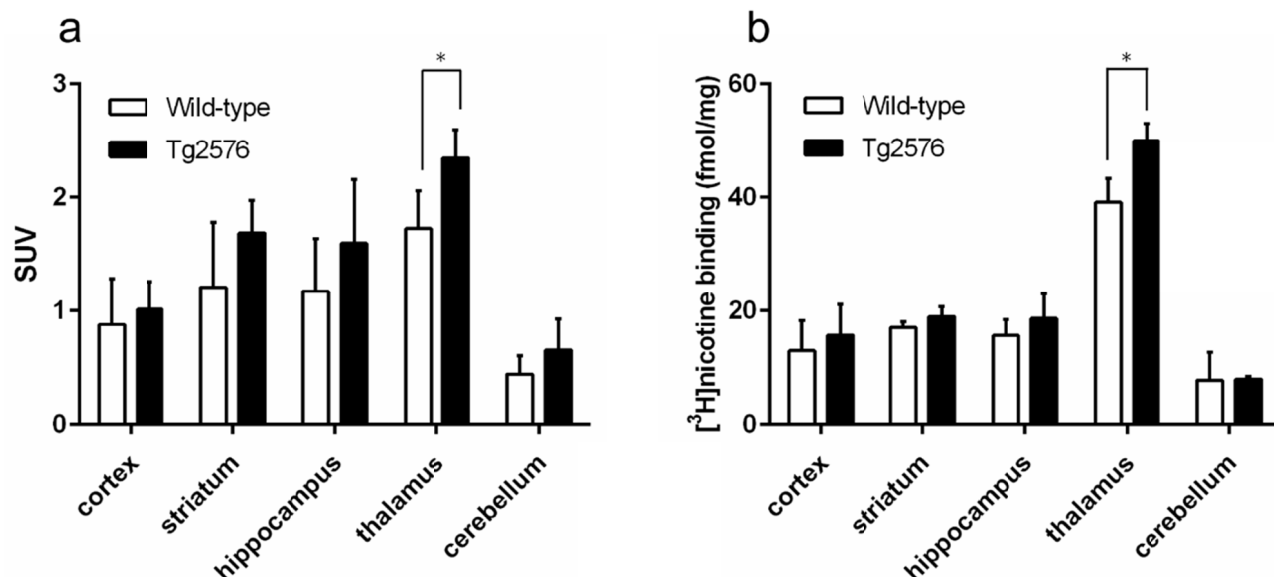


Figure 4. Changes in $[^{123}\text{I}]5\text{IA}$ binding and nAChR density in mouse model of Alzheimer's disease

(a) *In vivo* $[^{123}\text{I}]5\text{IA}$ -SPECT signal in brain regions of Tg2576 and wild-type mice. Each column represents an average of 4–5 mice and each bar represents the SD ($P < 0.05$ vs. wild-type). (b) Quantitative values of $[^3\text{H}]$ nicotine binding in each brain region of Tg2576 and wild-type mice 7 days after SPECT/CT imaging. Each column represents an average of 4–5 mice and each bar represents the SD ($P < 0.05$ vs. wild-type).